*Journal of Applied Fluid Mechanics*, Vol. 17, No. 1, pp. 273-283, 2024.
Available online at www.jafmonline.net, ISSN 1735-3572, EISSN 1735-3645.
https://doi.org/10.47176/jafm.17.1.1944

# Numerical Investigation of Oil–Air Flow Inside Tapered Roller Bearings with Oil Bath Lubrication

Z. Wang[1†], F. Wang[1], H. Duan[2,3], W. Wang[2], R. Guo[4] and Q. Yu[5]

[1]*School of Mechanical Engineering and Rail Transit, Changzhou University, Changzhou, China*
[2]*School of Mechatronics Engineering and Automation, Shanghai University, Shanghai, China*
[3]*Shanghai Bearing Technology Research Institute, Shanghai, China*
[4]*CRRC Qishuyan Institute CO,LTD., Changzhou, China*
[5]*AVIC Manufacturing Technology Institute, Beijing, China*

†*Corresponding Author Email: wangzhijian@cczu.edu.cn*

## ABSTRACT

Oil–air flow within an oil bath lubrication tapered roller bearing is essential for the lubrication and cooling of the bearing. In this paper, we develop a simulation model to investigate the flow field of tapered roller bearings with oil bath lubrication. The multiple reference frame (MRF) approach is used to describe the physical motion of the bearing, and the volume of fluid (VOF) two–phase flow model is used to track the oil–air interface in the flow field. The effects of mesh scale, geometric gap, and oil reservoir size on calculation time and convergence accuracy are examined in detail, and the effects of inner ring rotational speed and lubricant viscosity on frictional torque are systematically studied. The results of the numerical simulation indicate that as the gap distance between the raceway and the rolling elements decreases, the frictional torque is mainly generated by churning losses at the inner raceway and the rolling elements. The frictional torque increases with increasing inner ring speed and lubricating oil viscosity, with the rolling element contributing the largest portion at approximately 50% of the total. We demonstrate the effectiveness of a method to reduce frictional torque by optimizing the internal structure of the bearing to control oil flow. By optimizing the cage structure and reducing the roller half-cone angle, frictional torque can be reduced by 29.1% and 26.2%, respectively.

***Article History***

*Received April 17, 2023*
*Revised July 22, 2023*
*Accepted September 5, 2023*
*Available online November 1, 2023*

***Keywords:***

*Tapered roller bearings*
*Oil bath lubrication*
*Two-phase flow*
*Frictional torque*
*CFD simulation*

## 1. INTRODUCTION

With one–third of the world's energy resources being wasted in friction, wear, and corrosion (Holmberg & Erdemir, 2019), the ongoing energy crisis has led to an urgent need for improvements in the efficiency of transmission systems. Rolling bearings are important mechanical components that support rotational motion in machinery and in general are used for reducing friction. However, it has been shown (Matsuyama et al., 2004) that these bearings are the major contributors to power loss in some transmission systems. Therefore, reduction of the power loss due to rolling bearings is an important research topic.

Tapered roller bearings (TRB) are often applied to transmission systems due to their high loading capacity. However, with this type of roller bearing, sliding friction occurs at the flange-roller end, and oil flows from the small end to the large end owing to a "pumping effect". As a consequence, these bearing suffer from greater power loss compared with cylindrical roller bearings and ball bearings. There have been many studies (Raczyński, 1992; Liebrecht et al., 2015; Zhang et al., 2018) focusing on reduction of power loss in tapered roller bearing. The former has been well investigated and can be optimized by bearing kinematic performance analysis (Zhou & Hoeprich, 1991), while the latter has relied mainly on experimental tests, and some empirical models have been proposed based on the results of these tests (Marchesse et al., 2019). However, these models may not be reliable for predicting power losses when the geometry or operating conditions deviate from those of the experiments.

There have been a number of recent studies of lubricant flow behavior in rolling bearings based on computational fluid dynamics (CFD) simulations. Liu et al. (2023) developed a model combining the volume of fluid (VOF) method and dynamics to investigate the lubrication performance of oil–air two–phase flow in ball

bearings lubricated by lateral oil injection. They also examined the impact of cage clearance and ball relative motion on lubrication performance. Wei et al. (2022) focused on oil bath lubricated ball bearings and employed the MPS method to analyze the oil content and distribution of the bearings at different oil levels and rotational speeds. Kim and Jo (2018) conducted a study on the distribution of friction on the rolling elements of deep groove ball bearings. They established a simple analytical model to describe the internal fluid flow in these bearings. Morales-Espejel and Wemekamp (2022) introduced a robust theoretical framework for an engineering model designed to accurately calculate drag losses in rolling bearings. The efficacy of their model was confirmed through a meticulous comparison of its results with experimental measurements. Wen and Oshima (2014) developed a predictive method for bearing churning torque based on CFD analysis and demonstrated its applicability through experiments. Building upon this approach, they performed bearing optimization and successfully designed a ball bearing with significantly reduced torque. Hu et al. (2014) used the sliding mesh and VOF methods to analyze the oil–air flow within a ball bearing under oil jet lubrication. Gao et al. (2019a) developed a numerical method for estimating churning and drag losses in roller bearings and compared the results with those calculated by the SKF, Parker, and Palmgren models to demonstrate the validity of the method. Yan et al. (2016) investigated the effect of structure parameters on the flow distribution in high-speed ball bearings using Ansys Fluent commercial software. Concli et al. (2020) performed lubrication simulations on cylindrical roller bearings in the OpenFOAM environment, aiming to investigate lubricant distribution and the associated churning power losses. Maccioni et al. (2022) developed a CFD model of TRB that was able to take the aeration effect into consideration. In some of the above simulation studies, only part of the bearing was considered, owing to cyclic symmetry of the system. However, if nearby structures are considered, such as nozzles, the bearing system will no longer possess cyclic symmetry, and the used of simplified model based on the assumption of cyclic symmetry assumption would produce huge errors. In such cases, the model must consider the whole bearing. The commercial software STAR-CCM+ provides an overset grid approach to handle mesh topological variation and has been successfully applied to the study of gear engagement (Renjith et al., 2017). Therefore, in the present work, an attempt is made to apply the overset grid approach of STAR-CCM+ to investigate oil flow in TRB. Additionally, considering the quality of mesh elements, convergence of calculation, and computational efficiency, there is usually a gap distance between the raceway and the rolling element. Typically, this gap distance is achieved by reducing the dimensions of the rolling elements. However, from experience, it is common to reduce the diameter of the rolling element to between 85% and 99% of the original diameter (corresponding to gap distances of 0.05–0.5 mm) (Peterson et al., 2021b; Wu et al., 2016; Gao et al., 2019b), and few studies of rolling bearings have discussed this issue. Peterson, et al. (2021b) analyzed the impact of a reduced ball diameter on drag and determined that reducing the original ball diameter to 95% (with the gap between the ball and the raceway then being 0.16125 mm) yielded a satisfactory approximation, while also reducing the computational workload by approximately 80%. This amount of reduction was also adopted in a subsequent study (Peterson et al., 2021a), but it may not be suitable for TRB. The pumping properties of TRB may affect the selection of the gap. Sometimes, even though the gap does not influence frictional torque, it may affect flow distribution in the roller end. Some methods have been proposed to control oil flow. Various studies (Munro et al., 2007; Peterson et al., 2021a) have shown that rational cage optimization can reduce frictional torque, and the effectiveness of this approach has been experimentally verified. This method of structural optimization to control oil flow is not well adopted in TRB design, and it has not yet been the subject of any quantitative analysis through CFD simulation.

In the present work, numerical methods are used to investigate the oil–air flow inside TRB with oil bath lubrication. A quantitative analysis of the effects of different parameters on the frictional torque is performed and the underlying mechanisms of these effects are explored, with the ultimate aim of reducing frictional torque by optimizing the structure of TRB.

## 2. Model Setup and Numerical Method

### 2.1 Geometry

Table 1 lists the nominal dimensions of the TRB-LM48510 tapered roller bearing, which is used as a reference model for this study. The bearing is lubricated with an oil bath, as shown in Fig. 1. The dimensions of the oil reservoir are 200 mm in length, 80 mm in width, and 200 mm in height. The selection of oil reservoir dimensions will be discussed in Sec. 3.3.

**Table 1 Parameters of bearing**

| Parameter | Description | Value |
|---|---|---|
| *d* | Bore diameter | 34.925 mm |
| *D* | Outside diameter | 65.087 mm |
| *B* | Width | 18.034 mm |
| *N* | Number of rollers | 19 |
| *Cr* | Basic dynamic load rating | 71.6 kN |
| *C0r* | Basic static load rating | 84.3 kN |

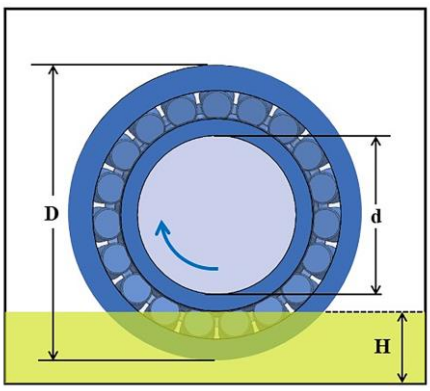


**Fig. 1 Geometry of the bearing model**

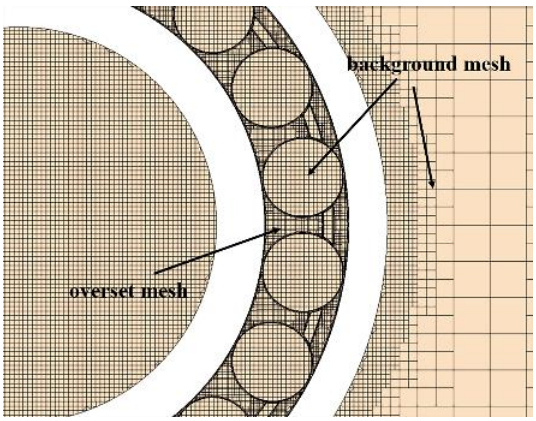


**Fig. 2 Overset mesh (overset and background)**

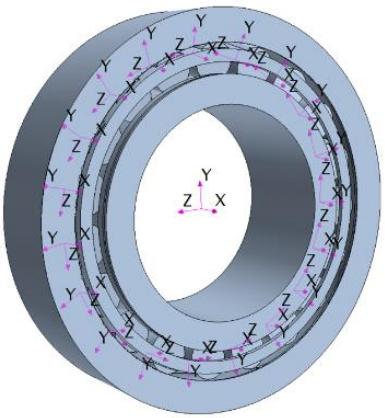

**Fig. 3 Establishment of the coordinate system**

### 2.2 Two-Phase Flow Model

The flow inside TRB with oil bath lubrication involves two phases, oil and air, and the flow interface of the liquid is constantly changing. The VOF model can accurately determine the position and shape of the two-phase interface.

When dealing with two-phase flow, let us assume that the volume fraction of the oil in the control body being calculated is $\varphi_{\text{oil}}$ : then, $\varphi_{\text{oil}}=0$ means that the oil phase is not present in the control body, $\varphi_{\text{oil}}=1$ means that only the oil phase is present in the control body, and $0<\varphi_{\text{oil}}<1$ indicates that there is an interface between the two phases in the control body (Hirt & Nichols, 1981). The definition of $\varphi_{\text{oil}}$ is thus as follows:

$$\begin{cases} \varphi_{\text{oil}}=0 & \text{air phase} \\ 0<\varphi_{\text{oil}}<1 & \text{interface(oil-air phase)} \\ \varphi_{\text{oil}}=1 & \text{oil phase} \end{cases} \tag{1}$$

The volume fraction of air $\varphi_{\text{air}}$ can be obtained from the constraint:

$$\varphi_{air}+\varphi_{oil}=1 \tag{2}$$

The interface between oil and air is tracked in the VOF model by solving the continuity equation for the volume fraction of the oil phase, which can be written as follows:

$$\frac{\partial}{\partial t}(\varphi_{\text{oil}}\rho_{\text{oil}})+\nabla\cdot(\varphi_{\text{oil}}\rho_{\text{oil}}\vec{v})=S_{a_{\text{oil}}} \tag{3}$$

where $\rho_{\text{oil}}$, $\vec{v}$, and $S_{a_{\text{oil}}}$ are the oil density, velocity vector, and mass source term (Ramdin & Henkes, 2012; Zhang et al., 2023).

### 2.3 Meshing Strategy

Overlapping grids (an overset mesh) (Renjith et al., 2017) are used for discretizing the multiple different grids that overlap each other in the computational domain. They have an advantage when dealing with complex motion problems involving multiple objects. The grid cells in an overlapping grid consist of active cells, receptor cells, and inactive cells. Active cells are used to solve the discrete control equations, while inactive cells are excluded from the equation-solving process. Receptor cells are connected to the boundaries of the overset region and serve to separate active and inactive cells in the background region. This study presents the segmentation of the tapered roller bearings' domain using the overset mesh and background mesh definitions depicted in Fig. 2. Given the intricate nature of the bearing structure, we opted to use a Trimmed Cell Mesher approach for discretizing the flow field. The overset region includes three layers of prismatic mesh, which is much finer than the mesh used in other areas. Additionally, to prevent the mesh surface from being incorrectly connected, a set of contact guards is placed between the cage and the roller. A minimum of three grid layers per gap is required to meet the precision requirement for grid partitioning. Moreover, the dimensionless wall distance $y^+$ falls within the range of 4.57– 8.31 in all cases.

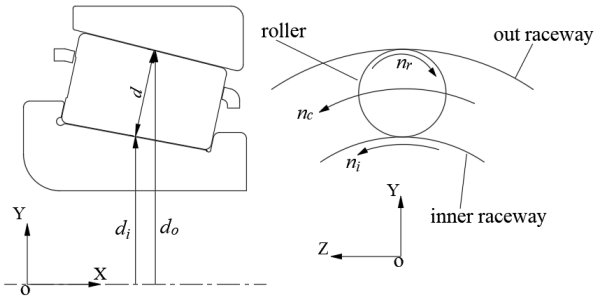


**Fig. 4 Schematic diagram of tapered roller bearing**

### 2.4 Boundary Conditions

The MRF approach is employed to describe the physical motion of the bearings. Referring to Fig. 3, a global coordinate system is adopted for the inner ring, outer ring, and cage, while the rollers rotate about their local reference frames as well as in the global reference frame. The inner ring is driven, while the outer ring remains fixed. The outer surface of the oil reservoir is also fixed, and its boundary condition is taken as a wall boundary. Figure 4 is a schematic of TRB. The inner ring speed is $n_i$. From motion analysis, it is found that the

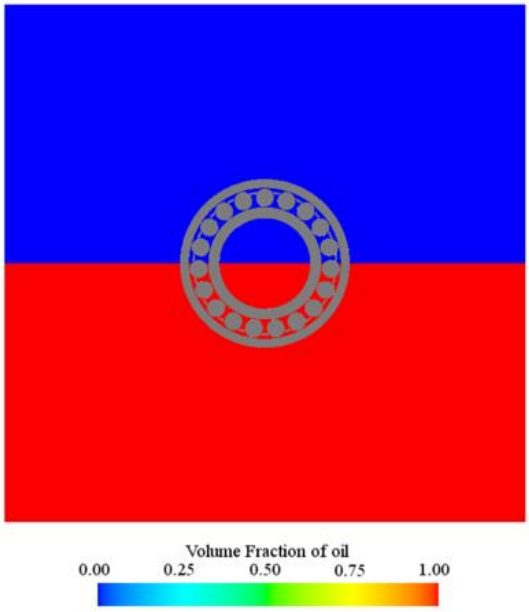


**Fig. 5 Field function sets the initial oil level**

speed of revolution of the rollers $n_c$, their speed of rotation $n_r$, and the cage speed $n_{cage}$ satisfy the following equations:

$$n_c = n_{cage} = n_i \frac{d_i}{d_o + d_i} \tag{4}$$

$$n_r = n_c \frac{d_o}{d} \tag{5}$$

### 2.5 Solution Method

The governing equations utilized in STAR-CCM+ to depict turbulent flow rely on numerical solution of the Reynolds–averaged Navier–Stokes (RANS) equations through the finite volume method. The choice of the shear stress transport (SST) *k-ω* turbulence model in STAR-CCM+ is due to its applicability under a wide range of Reynolds numbers and its incorporation of the advantages of both the *k-ε* and *k-ω* models. It provides precise forecasts of adverse pressure gradient flow and boundary layer flow, while maintaining robustness in complex geometries and rotating flows (Eleni et al., 2012; Menter, 2019). Gravity is added to the physical model in the $-y$ direction and is set as [0, −9.81, 0] m/s$^2$ in the initial conditions. In Fig. 5, the field function is used to set the initial oil level. The oil level is selected to be at the centerline ($H$ = 100 mm), covering half of the bearing.

To obtain the frictional torque of each component, the shear stress and pressure force have to be integrated over the surfaces:

$$\overrightarrow{M_F} = (\overrightarrow{F_t} + \overrightarrow{F_n}) \times \vec{r} = \left( \int_A (\tau + p) \cdot \vec{n} \, dA \right) \times \vec{r} \tag{6}$$

where $\overrightarrow{M_F}$, $\overrightarrow{F_t}$, $\overrightarrow{F_n}$, $\vec{n}$, $\vec{r}$, $p$, and $\tau$ are the total torque vector, viscous force vector, pressure force vector, surface normal vector, position vector, pressure forces, and shear stresses.

**Table 2 Comparison of results with different mesh number**

| Mesh number | computation time (h) | Frictional torque (N·mm) | Relative difference |
|---|---|---|---|
| 2,153,585 | 18.74 | 9.798 | 21.0% |
| 2,830,603 | 27.47 | 10.585 | 14.7% |
| 3,106,402 | 29.29 | 12.271 | 1.06% |
| 3,623,907 | 35.68 | 12.387 | 0.13% |
| 4,105,926 | 48.27 | 12.403 | / |

In this study, a full-scale model is simulated under different operating conditions, with inner ring speeds ranging from 500 to 8000 rpm, fluid viscosities ranging from 32 to 68 mm$^2$/s, and a density of 860 kg/m$^3$. The appropriate time step is determined by the ratio between the minimum mesh size and the characteristic flow velocity. A starting time step of $10^{-4}$s and a minimum time step size of $10^{-5}$ s are suitable for most cases.

## 3. Results and Discussion

### 3.1 Grid Study

The finer the grid partitioning, the higher is the accuracy of the solution. Moreover, after a certain number of grids, the improvement in calculational accuracy is not significant. Therefore, it is necessary to determine the appropriate number of grids to obtain accurate results at a lower computational cost. During simulation, eight-core parallel computing is used, with an inner ring speed of 1000 rpm and a kinematic viscosity of 50 mm$^2$/s. Table 2 presents information on the mesh number, simulation time, frictional torque values, and their respective relative differences when compared with the results obtained for the finest mesh. The simulation time is evaluated as the time at which a convergence stopping criterion is reached such that the frictional torque approaches stability. From Table 2, it can be observed that as mesh number increases, the frictional torque first increases and then tends to a constant value, while the simulation time sharply increases. Thus, under the current working conditions, the best choice is to have the number of cells equal to 3,106,402. The corresponding basic mesh size is 7% of the rolling element diameter (0.5 mm), and the global mesh size varies from 0.1 mm to 0.8 mm. In this case, the relative difference in frictional torque is less than 1.06%, and the simulation time can be reduced by nearly 40%.

### 3.2 Gap Study

The use of excessively small unit grids in the solution process results in a significant consumption of computation time, which is undesirable. Hence, it is necessary to explore various gap sizes. By striking a balance between computational efficiency and accuracy, we can determine the optimal gap distance.

Varying the proportion of the original rolling element diameter leads to different gap values. In this study, the proportion of the original rolling element diameter ranges from 86.4% to 98.6% (corresponding to gap distances between the raceway and the rolling element of 0.05–

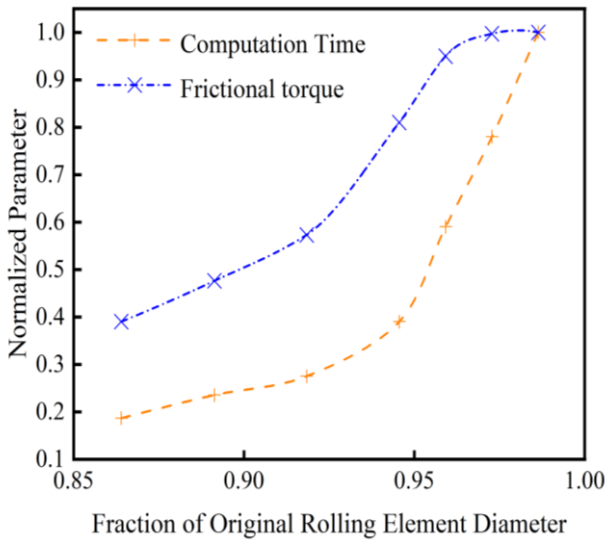


**Fig. 6 Effect of different fractions of original rolling element diameter on frictional torque and computation time. (The parameters are normalized by the maximum predicted value for the original rolling element diameter)**

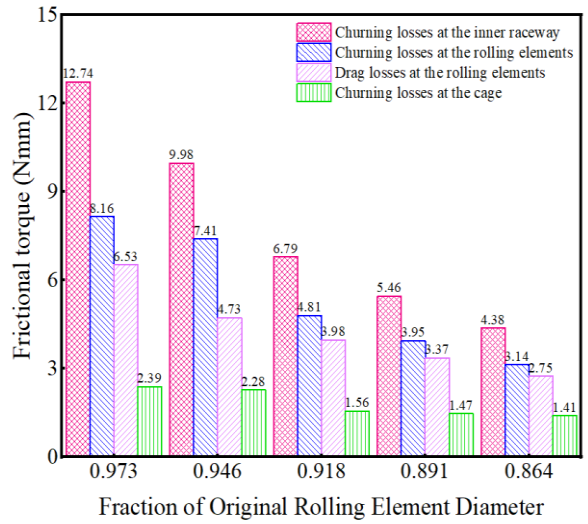


**Fig. 7 Effect of different fractions of original rolling element diameter on the components of frictional torque**

0.5mm), as shown in Fig. 6, which illustrates the impact of different proportions of the original rolling element diameter on frictional torque and computation time. When the proportion of the original rolling element diameter is 95.9%, the computational workload is reduced by approximately 41%, and the error in frictional torque is only 5% compared with the case where the proportion of the original rolling element diameter is 98.6%. Therefore, considering the trade-off between computational efficiency and accuracy, a proportion of the original rolling element diameter of 95.9% (corresponding to a gap distance of 0.15 mm between the raceway and the rolling element) will be used for the subsequent calculations.

The use of the CFD model enables calculation of load-independent losses and analysis of the effect of various bearing components on the frictional torque. From Fig. 7, it is evident that the proportion of the original rolling element diameter has a significant impact on the components of frictional torque. As the proportion of the original rolling element diameter increases (and correspondingly the gap distance between the raceway and the rolling elements decreases), the frictional torque is primarily caused by churning losses at the inner raceway and the rolling elements. Figure 8 demonstrates that with an increase in the proportion of the original rolling element diameter, the shear forces on both the inner raceway and the rolling elements increase, ultimately leading to an increase in shear stress. In fact, the churning losses are mainly caused by the shear stress of the lubricants, which is the reason for the increase in total frictional torque.

### 3.3 Oil Reservoir Size Study

It is known from experience that obstacles near moving components immersed in the oil bath can greatly affect the motion in the bath. Hence, it is essential to investigate how varying the oil reservoir size affects the computational results in this study. From Fig. 9, it can be observed that the frictional torque of the #3 oil reservoir

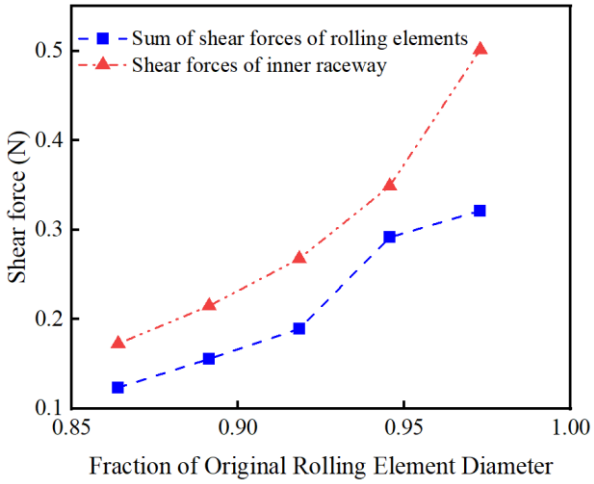


**Fig. 8 Shear force of the inner raceway and the rolling elements for different fractions of the original rolling element diameter**

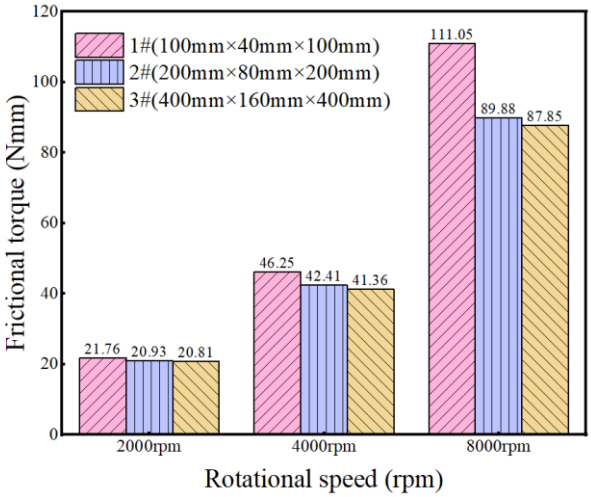


**Fig. 9 Influence of different oil reservoir sizes on calculation results**

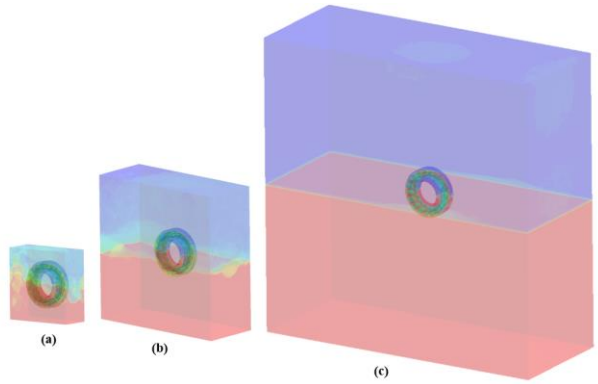


**Fig. 10 Oil volume fraction for different oil reservoir sizes at 4000 rpm. (a) 1# 100×40×100 mm$^3$, (b) 2# 200×80×200 mm$^3$, (c) 3# 400×160×400 mm$^3$**

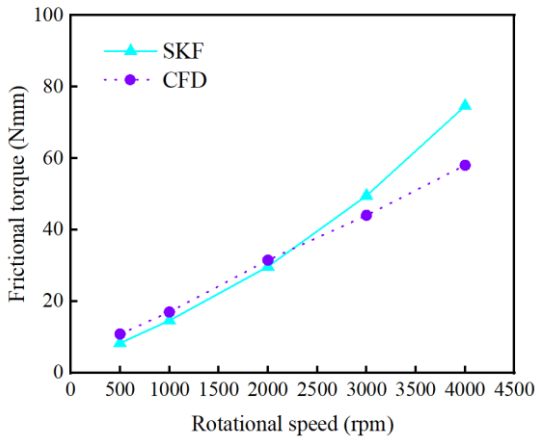


**Fig. 11 Comparison of frictional torque between CFD simulation and SKF model at different speeds**

decreased by 4.4%, 10.6%, and 20.9% compared with that of the #1 oil reservoir at 2000 rpm, 4000 rpm, and 8000 rpm, respectively. Thus, the oil reservoir size has an effect on the calculation of the frictional torque, with this effect becoming increasingly significant at higher speeds. Figure 10 illustrates the distribution of oil volume in various oil reservoir models at 4000 rpm. It can be seen that with an oil reservoir that is too small, the motion of the oil will be impeded. Selecting the #2 oil reservoir can be considered a reasonable choice, since it leads to only a small error compared with the best case, namely, the #3 reservoir.

### 3.4 Influence of the Inner Ring Rotational Speed

We compare our CFD simulation results with those from the standard SKF empirical model. The results, presented in Fig. 11, reveal a satisfactory agreement between our simulation and the SKF model at rotational speeds below 2300 rpm. Nevertheless, with increasing rotational speed, the difference between the frictional torque predicted by the SKF model and that from the simulation becomes more significant, with the SKF model predicting a higher frictional torque. This finding is consistent with that of Feldermann et al. (2017).

Table 3 shows the distribution of load-independent losses for components of TRB. It can be observed that as the rotational speed increases, the proportion of the churning losses at the rolling elements decreases slightly, while other losses increase slightly. Rolling elements account for the highest percentage of losses, with the combined churning and drag losses making up approximately 50.2%. Churning losses generated by the inner raceway represent 37.0% of the total losses, while the cage accounts for the smallest churning losses at approximately 12.8%.

As can be seen from Figs. 12 and 13, the oil volume fraction at large ends of the rollers decreases as the rotational speed increases. This can be attributed to the pumping effect that moves the lubricating oil from the small end to the large end, combined with the centrifugal force produced by the rotation of the rollers, which throws out the majority of the lubricating oil from the top. This process is illustrated in Fig. 14.

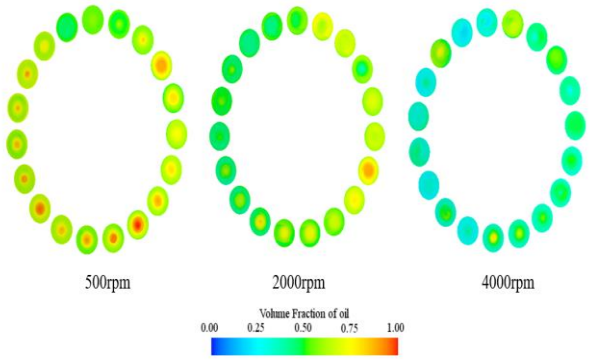


**Fig. 12 Oil volume fraction at the large ends of the rollers for different rotational speeds**

**Table 3 Distribution of power loss in components at different rotational speeds**

| | | Rotational speed (rpm) | | | | |
|---|---|---|---|---|---|---|
| Component | Type of power loss | 500 | 1000 | 2000 | 3000 | 4000 |
| Rolling element | Churning losses | 31.21% | 30.30% | 29.94% | 28.34% | 27.45% |
| Rolling element | Drag losses | 19.74% | 20.08% | 20.23% | 21.45% | 22.09% |
| Inner raceway | Churning losses | 36.70% | 36.88% | 36.92% | 37.13% | 37.35% |
| Cage | Churning losses | 12.35% | 12.74% | 12.91% | 13.08% | 13.11% |

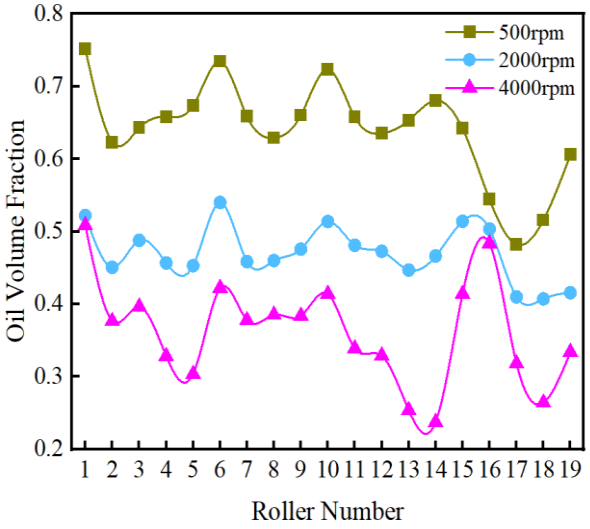


**Fig. 13 Average oil volume fraction at the large ends of the rollers for different rotational speeds**

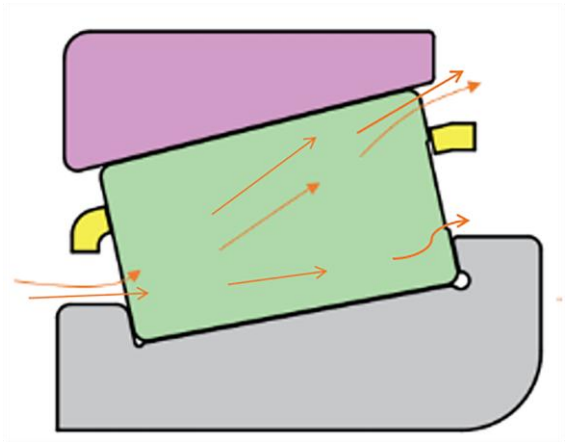

**Fig. 14 Flow of lubricating oil caused by pumping effect**

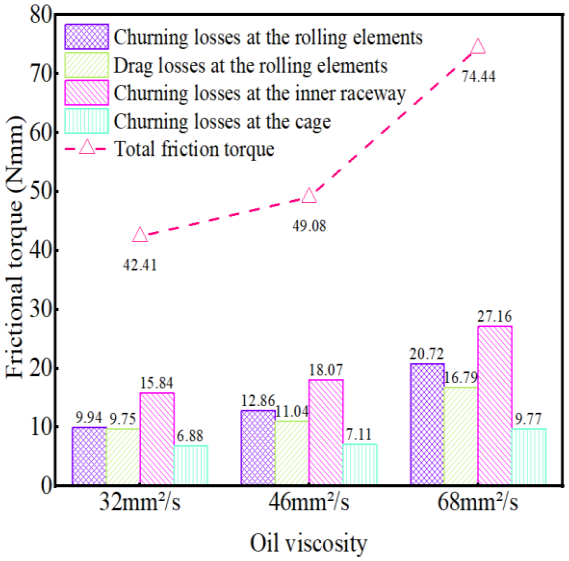


**Fig. 15 Effect of oil viscosity on components of frictional torque at 4000 rpm**

### 3.5 Influence of Oil Viscosity

Figure 15 shows the impact of various lubricant viscosities on the frictional torque at a constant rotational speed. The results indicate a positive correlation between the total frictional torque and the viscosity of the lubricant. Compared with the total frictional torque at a viscosity of 32 $mm^2/s$, the total frictional torque at viscosities of 46 $mm^2/s$ and 68 $mm^2/s$ increased by 15.7% and 75.5%, respectively, the churning losses caused by the rolling elements increased by 29.4% and 108.5%, the churning losses of the raceway increased by 14.1% and 71.5%, the drag losses of the rolling elements increased by 13.2% and 72.2%, and the churning losses of the cage increased by 3.3% and 42.0%. Thus, variations in the viscosity have their greatest influence on the churning losses associated with the rolling elements. Figure 16 shows the pressure and velocity vectors around a rolling element for various lubricant viscosities. It can be seen that an increase in the viscosity leads to a decrease in fluid velocity within the bearing chamber and an increase in pressure. Notably, significant high-pressure zones occur at the contact of the rollers with the inner and outer rings and cage, resulting in larger churning and drag losses.

Figure 17 illustrates the impact of lubricating oil viscosity on frictional torque at different rotational speeds. Increasing the rotational speed leads to an increase in total frictional torque. At low viscosity, the relationship between rotational speed and frictional torque is nearly linear, whereas at high viscosity, the frictional torque rises steeply with increasing rotational speed.

Figure 18 shows the volume fraction of lubricating oil at the raceway at a rotational speed of 8000 rpm for oils with viscosities of 32 $mm^2/s$ and 68 $mm^2/s$, respectively. It can be seen that with the high-viscosity oil, there is lubrication starvation at the raceway. Therefore, it is recommended that to ensure reliable lubrication under high-speed working conditions, low-viscosity lubricating oils should be chosen.

## 4. Optimization of Bearing Internal Geometry

### 4.1 Cage Design

The load-independent frictional torque of TRB is largely determined by the flow of lubricating oil from the small ends of the rollers to the large ends caused by the pumping effect. If this oil flow can be controlled or the pumping effect can be reduced, it may be possible to reduce the load-independent frictional torque. Figure 19 shows a cage design in which the cage's left guard is extended toward the inner ring. This may hinder the flow of lubricating oil into the bearing chamber from the small end of the roller. Figure 20 illustrates the volume distribution of lubricating oil on the surface of the rolling element before and after the improvement. It can be observed that the volume fraction of the improved rolling element surface is significantly reduced. This will lead to a decrease in the total frictional torque, and indeed, as shown in Fig. 21, the frictional torque is reduced by about 29.1%.

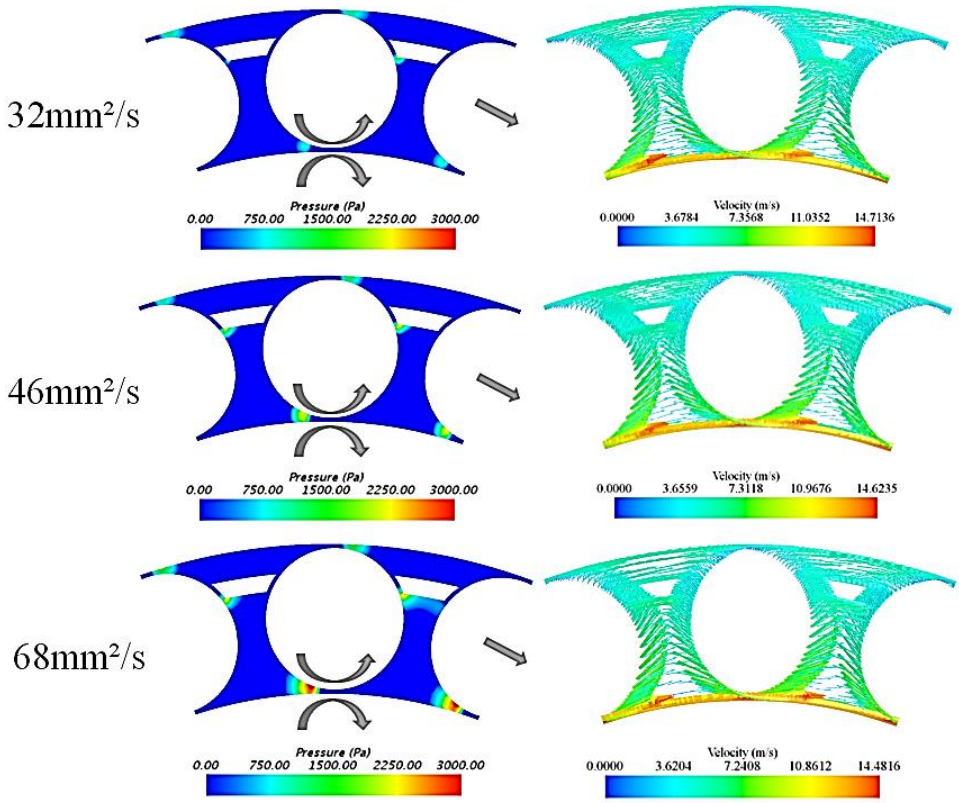


**Fig. 16 Pressure and velocity vectors around a rolling element for different lubricant viscosities at 4000 rpm**

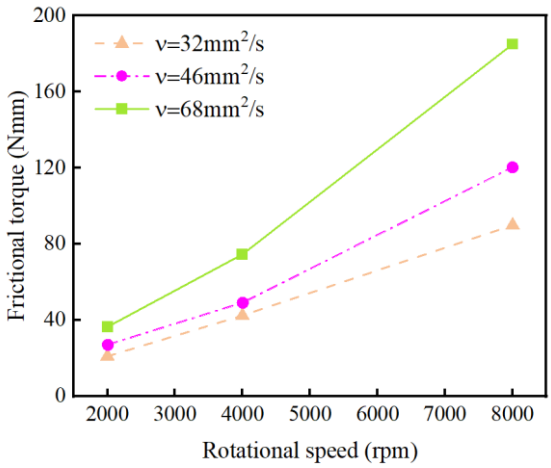


**Fig. 17 Influence of viscosity and rotational speed on frictional torque**

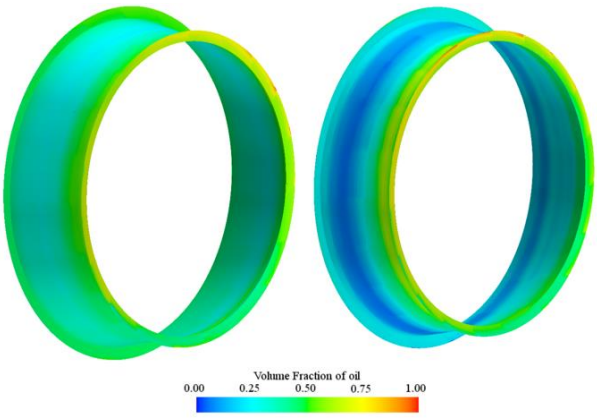


**Fig. 18 Oil volume fraction at raceway for different viscosities at 8000 rpm**

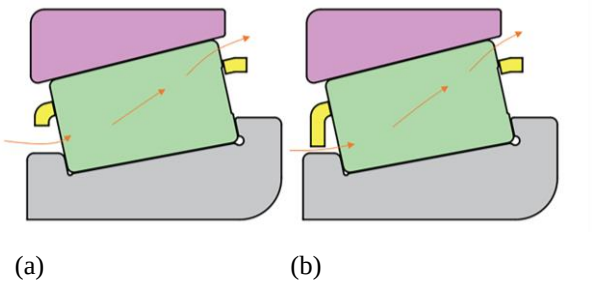


**Fig. 19 (a) Cage before improvement. (b) Improved cage**

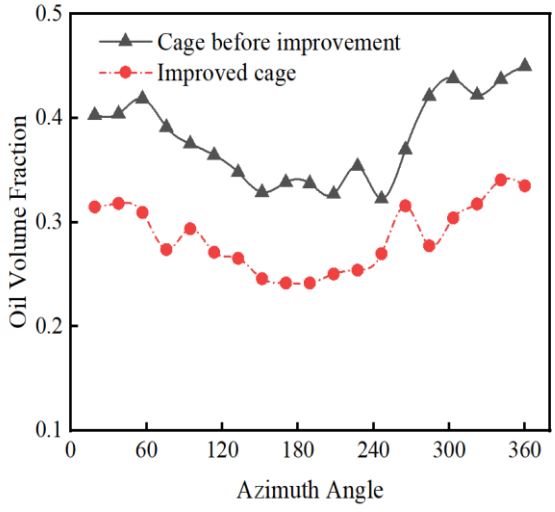


**Fig. 20 Distribution of average oil volume fraction on surface of rolling element for different cages**

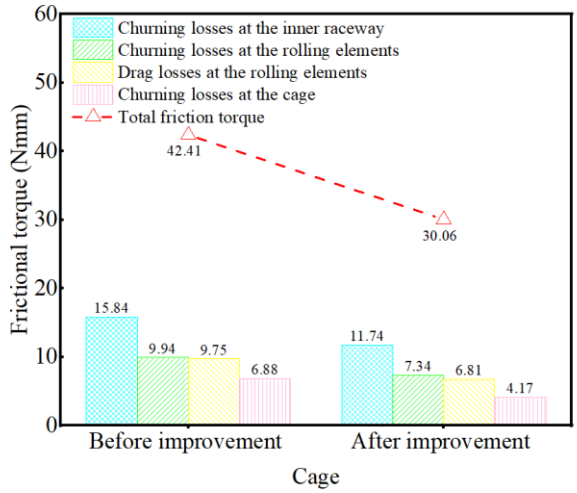


**Fig. 21 Effect of different cages on components of frictional torque**

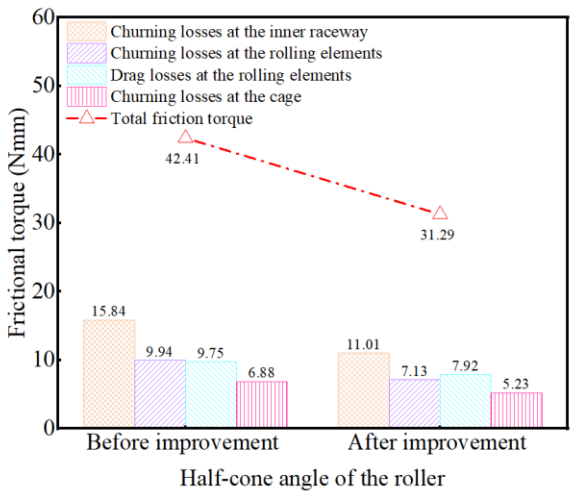


**Fig. 24 Effect of different roller half-cone angles on components of frictional torque**

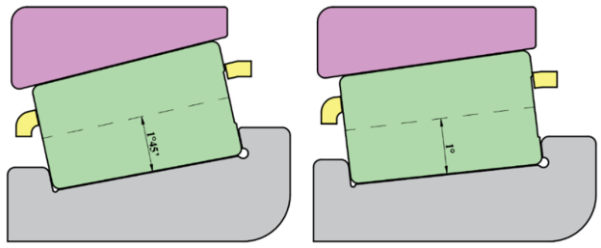


**Fig. 22 (a) Roller half-cone angle before improvement. (b) Improved roller half-cone angle**

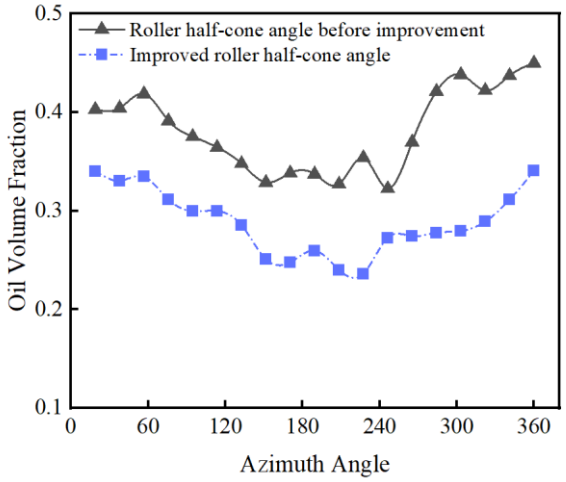


**Fig. 23 Distribution of average oil volume fraction on surface of rolling element for different roller half-cone angles**

### 4.2 Roller Half-Cone Angle Design

Figure 22 shows the effect of decreasing the roller half-cone angle from its original value of 1°45′ to 1°. The roller half-cone angles of 1°45' and 1° correspond to contact angles of 14°5' and 10°, respectively. The typical range for contact angles is between 10° and 30°, which ensures the bearing capacity. This change in roller half-cone angle leads to corresponding changes in the cone angles of the inner and outer rings. However, the length of the roller, the diameter of the bearing's pitch circle, and the number of rollers remain unchanged. Reducing the roller half-cone angle can effectively decrease the pumping effect. Figure 23 demonstrates that as the roller half-cone angle decreases, the oil volume fraction on the roller surfaces also decreases, resulting in a decrease in both the total frictional torque and its individual components. In addition, Fig. 24 shows that the total frictional torque is reduced by 26.2% under these conditions. Therefore, reducing the roller half-cone angle will help to reduce the load-independent frictional torque of TRB. It is important to highlight that decreasing the roller half-cone angle may result in a reduction of the axial bearing capacity of TRB. Therefore, when designing the internal structure of such bearings, a comprehensive approach should be adopted.

## 5. CONCLUSION

We have developed a CFD simulation model to investigate the flow fields of TRB with oil bath lubrication. The effects of mesh scale, geometrical gap, and oil reservoir size on the computation time and convergence accuracy have been examined in detail. Our simulation results have been compared with the values from the SKF empirical model. The effects of inner ring speed and lubricating oil viscosity on frictional torque have been systematically studied. Methods have been proposed to reduce the frictional torque, including changing the cage structure and reducing the roller half-cone angle. Our specific conclusions are as follows:

1. In simulation models of TRB, the choice of the geometric gap requires a trade-off between accuracy and computation time. For the operating conditions considered here, 0.15 mm (95.9% of the original rolling element diameter) is the most appropriate gap distance. As the gap distance between the raceway and the rolling elements decreases, the frictional torque is mainly generated by

churning losses at the inner raceway and the rolling elements.

2. The small size of the oil reservoir has an impact on the calculation of frictional torque, and this impact becomes increasingly significant at higher speeds.

3. The load-independent frictional torque of TRB is proportional to the inner ring speed, and increases with speed. Among the frictional torque components, the frictional torque due to the rolling elements is the largest, accounting for about 50% of the total.

4. As the lubricating oil viscosity increases, the load-independent frictional torque on TRB increases. In addition, our model shows that lubricant starvation will occur on the raceway surface at high speeds. Therefore, to ensure reliable lubrication, it is recommended to choose low-viscosity lubricating oils for high-speed working conditions.

5. Through optimized design of the cage structure and roller half-cone angle, the total frictional torque can be reduced by 29.1% and 26.2%, respectively.

In future work, the performance of TRB will be comprehensively evaluated in combination with the temperature field.

## AUTHORS CONTRIBUTION

**Zhijian Wang**: Conceptualization; Data collection; Visualization; Writing – original draft. **Fei Wang**: Writing – original draft (Supporting); Conceptualization (supporting); Writing – review and editing. **Hongyu Duan**: Supervision, Writing – review and editing. Wen Wang: Writing – Review. **Rubing Guo**: Writing – Review. **Qingtao Yu**: Writing – Review.

## CONFLICT OF INTEREST

The authors declare that they have no competing interests.

## ACKNOWLEDGEMENT

The funding for this study is provided by the Natural Science Fund for Colleges and Universities in Jiangsu Province (No. 20KJD460002) and the Changzhou Science and Technology Plan Project (No. CJ20220129). The authors express their appreciation for the resources received from Changzhou University's High Performance Computation Laboratory.

## REFERENCES

Concli, F., Schaefer, C. T., & Bohnert, C. (2020). Innovative meshing strategies for bearing lubrication simulations. *Lubricants*, *8*, 46. http://doi.org/10.3390/lubricants8040046

Eleni, D. C., Athanasios, T. I., & Dionissios, M. P. (2012). Evaluation of the turbulence models for the simulation of the flow over a National Advisory Committee for Aeronautics (NACA) 0012 airfoil. *Journal of Mechanical Engineering Research*, 4. http://doi.org/10.5897/jmer11.074

Feldermann, A., Fischer, D., Neumann, S., & Jacobs, G. (2017). Determination of hydraulic losses in radial cylindrical roller bearings using CFD simulations. *Tribology International*, *113*, 245–251. https://doi.org/10.1016/j.triboint.2017.03.020

Gao, W., Lyu, Y., Liu, Z., & Nelias, D. (2019a). Validation and application of a numerical approach for the estimation of drag and churning losses in high speed roller bearings. *Applied Thermal Engineering*, *153*, 390–397. http://doi.org/10.1016/j.applthermaleng.2019.03.028

Gao, W., Nelias, D., Li, K., Liu, Z., & Lyu, Y. (2019b). A multiphase computational study of oil distribution inside roller bearings with under-race lubrication. *Tribology International*, *140*, 105862. http://doi.org/10.1016/j.triboint.2019.105862

Hirt, C., & Nichols, B. (1981). Volume of fluid (VOF) method for the dynamics of free boundaries. *Journal of Computational Physics*, *39* (1), 201–225. https://doi.org/10.1016/0021-9991(81)90145-5

Holmberg, K., & Erdemir, A. (2019). The impact of tribology on energy use and $CO_2$ emission globally and in combustion engine and electric cars. *Tribology International*, *135*, 389–396. http://doi.org/10.1016/j.triboint.2019.03.024

Hu, J., Wu, W., Wu, M., & Yuan, S. (2014). Numerical investigation of the air–oil two-phase flow inside an oil-jet lubricated ball bearing. *International Journal of Heat and Mass Transfer*, *68*, 85–93. http://doi.org/10.1016/j.ijheatmasstransfer.2013.09.013

Kim, C. H., & Jo, J. H. (2018). Fluid flow analysis for friction torque around rolling element in ball bearings. *Journal of Friction and Wear*, *38*, 424–429. http://doi.org/10.3103/s106836661706006x

Liebrecht, J., Si, X., Sauer, B., & Schwarze, H. (2015). Investigation of drag and churning losses on tapered roller bearings. *Strojniški vestnik – Journal of Mechanical Engineering*, *61*, 399–408. http://doi.org/10.5545/sv-jme.2015.2490

Liu, J., Ni, H., Zhou, R., Li, X., Xing, Q., & Pan, G. (2023). A simulation analysis of ball bearing lubrication characteristics considering the cage clearance. *Journal of Tribology*, *145*, 044301–1. http://doi.org/10.1115/1.4056358

Maccioni, L., Chernoray, V. G., Mastrone, M. N., Bohnert, C., & Concli, F. (2022). Study of the impact of aeration on the lubricant behavior in a tapered roller bearing: Innovative numerical modelling and validation via particle image velocimetry. *Tribology International*, *165*, 107301. http://doi.org/10.1016/j.triboint.2021.107301

Marchesse, Y., Changenet, C., & Ville, F. (2019). Drag power loss investigation in cylindrical roller bearings

using CFD approach. *Tribology Transactions 62*, 403-411. http://doi.org/10.1080/10402004.2018.1565009

Matsuyama, H., Dodoro, H., Ogino, K., Ohshima, H., & Toda, H. (2004). Development of super-low friction torque tapered roller bearing for improved fuel efficiency. *SAE Technical*, *01*, 2674. http://doi.org/https://doi.org/10.4271/2004-01-2674

Menter, F. R. (2009). Review of the shear-stress transport turbulence model experience from an industrial perspective. *International Journal of Computational Fluid Dynamics*, *23*, 305-316. http://doi.org/10.1080/10618560902773387

Morales-Espejel, G. E., & Wemekamp, A. W. (2022). An engineering drag losses model for rolling bearings. *Proceedings of the Institution of Mechanical Engineers, Part J: Journal of Engineering Tribology*, *237*, 415–430. http://doi.org/10.1177/13506501221117959

Munro, G., Watters, R., & Roberts, E. (2007, September 19–21). *The impact of cage design on ball bearing torque behaviour*. Proc. 12th ESMATS, Liverpool, UK. https://esmats.eu/esmatspapers/pastpapers/pdfs/2007/munro.pdf

Peterson, W., Russell, T., Sadeghi, F., & Berhan, M. T. (2021a). Experimental and analytical investigation of fluid drag losses in rolling element bearings. *Tribology International*, *161*, 107106. http://doi.org/10.1016/j.triboint.2021.107106

Peterson, W., Russell, T., Sadeghi, F., Berhan, M. T., Stacke, L.-E., & Ståhl, J. (2021b). A CFD investigation of lubricant flow in deep groove ball bearings. *Tribology International*, *154*, 106735. http://doi.org/10.1016/j.triboint.2020.106735

Raczyński, A. (1992). Effect of working surface shape on power loss in taper roller bearings. *Wear*, *152*, 31–45. http://doi.org/https://doi.org/10.1016/0043-1648(92)90202-J

Ramdin, M., & Henkes, R. (2012). Computational fluid dynamics modeling of Benjamin and Taylor bubbles in two-phase flow in pipes. *Journal of Fluids Engineering ASME*, *134*(4), 1–8. https://doi.org/10.1115/1.4006405

Renjith, S., Srinivasa, V. K., & Venkateshaiah, U. (2017). Thermal performance prediction of jet lubricated transmission system using computational methods. *SAE Technical Paper Series*, *01*, 2437. http://doi.org/10.4271/2017-01-2437

Wei, C., Wu, W., Hou, X., & Yuan, S. (2022). Study on oil distribution and oil content of oil bath lubrication bearings based on MPS method. *Tribology Transactions*, *65*, 942–951. http://doi.org/10.1080/10402004.2022.2113193

Wen, Y., & Oshima, S. (2014). Oil flow simulation based on CFD for reducing agitation torque of ball bearings. *SAE International Journal of Passenger Cars - Mechanical Systems*, *7*, 1385–1391. http://doi.org/10.4271/2014-01-2850

Wu, W., Hu, C., Hu, J., & Yuan, S. (2016). Jet cooling for rolling bearings: Flow visualization and temperature distribution. *Applied Thermal Engineering*, *105*, 217–224. http://doi.org/10.1016/j.applthermaleng.2016.05.147

Yan, K., Zhang, J., Hong, J., Wang, Y., & Zhu, Y. (2016). Structural optimization of lubrication device for high speed angular contact ball bearing based on internal fluid flow analysis. *International Journal of Heat and Mass Transfer*, *95*, 540–550. http://doi.org/10.1016/j.ijheatmasstransfer.2015.12.036

Zhang, C., Gu, L., Mao, Y., & Wang, L. (2018). Modeling the frictional torque of a dry-lubricated tapered roller bearing considering the roller skewing. *Friction*, *7*, 51–563. http://doi.org/10.1007/s40544-018-0232-8

Zhang, J. J., Lu, L. M., Zheng, Z. Y., Gan, L., & Lv, Z. Y. (2023). Visual comparative analysis for the oil-air two-phase flow of an oil-jet lubricated roller-sliding bearing. *Journal of Applied Fluid Mechanics*, *16*, 179−191. http://doi.org/10.47176/jafm.16.01.1345

Zhou, R. S., & Hoeprich, M. R. (1991). Torque of Tapered Roller Bearings. *Journal of Tribology*, *113*, 590–597. http://doi.org/https://doi.org/10.1115/1.2920664